Measurement of the Differential q^2 Spectrum and Forward-Backward Asymmetry for $B \to K^{(*)}\ell^+\ell^-$

K. Abe,[10] K. Abe,[46] N. Abe,[49] I. Adachi,[10] H. Aihara,[48] M. Akatsu,[24] Y. Asano,[53] T. Aso,[52] V. Aulchenko,[2] T. Aushev,[14] T. Aziz,[44] S. Bahinipati,[6] A. M. Bakich,[43] Y. Ban,[36] M. Barbero,[9] A. Bay,[20] I. Bedny,[2] U. Bitenc,[15] I. Bizjak,[15] S. Blyth,[29] A. Bondar,[2] A. Bozek,[30] M. Bračko,[22,15] J. Brodzicka,[30] T. E. Browder,[9] M.-C. Chang,[29] P. Chang,[29] Y. Chao,[29] A. Chen,[26] K.-F. Chen,[29] W. T. Chen,[26] B. G. Cheon,[4] R. Chistov,[14] S.-K. Choi,[8] Y. Choi,[42] Y. K. Choi,[42] A. Chuvikov,[37] S. Cole,[43] M. Danilov,[14] M. Dash,[55] L. Y. Dong,[12] R. Dowd,[23] J. Dragic,[23] A. Drutskoy,[6] S. Eidelman,[2] Y. Enari,[24] D. Epifanov,[2] C. W. Everton,[23] F. Fang,[9] S. Fratina,[15] H. Fujii,[10] N. Gabyshev,[2] A. Garmash,[37] T. Gershon,[10] A. Go,[26] G. Gokhroo,[44] B. Golob,[21,15] M. Grosse Perdekamp,[38] H. Guler,[9] J. Haba,[10] F. Handa,[47] K. Hara,[10] T. Hara,[34] N. C. Hastings,[10] K. Hasuko,[38] K. Hayasaka,[24] H. Hayashii,[25] M. Hazumi,[10] E. M. Heenan,[23] I. Higuchi,[47] T. Higuchi,[10] L. Hinz,[20] T. Hojo,[34] T. Hokuue,[24] Y. Hoshi,[46] K. Hoshina,[51] S. Hou,[26] W.-S. Hou,[29] Y. B. Hsiung,[29] H.-C. Huang,[29] T. Igaki,[24] Y. Igarashi,[10] T. Iijima,[24] A. Imoto,[25] K. Inami,[24] A. Ishikawa,[10] H. Ishino,[49] K. Itoh,[48] R. Itoh,[10] M. Iwamoto,[3] M. Iwasaki,[48] Y. Iwasaki,[10] R. Kagan,[14] H. Kakuno,[48] J. H. Kang,[56] J. S. Kang,[17] P. Kapusta,[30] S. U. Kataoka,[25] N. Katayama,[10] H. Kawai,[3] H. Kawai,[48] Y. Kawakami,[24] N. Kawamura,[1] T. Kawasaki,[32] N. Kent,[9] H. R. Khan,[49] A. Kibayashi,[49] H. Kichimi,[10] H. J. Kim,[19] H. O. Kim,[42] Hyunwoo Kim,[17] J. H. Kim,[42] S. K. Kim,[41] T. H. Kim,[56] K. Kinoshita,[6] P. Koppenburg,[10] S. Korpar,[22,15] P. Križan,[21,15] P. Krokovny,[2] R. Kulasiri,[6] C. C. Kuo,[26] H. Kurashiro,[49] E. Kurihara,[3] A. Kusaka,[48] A. Kuzmin,[2] Y.-J. Kwon,[56] J. S. Lange,[7] G. Leder,[13] S. E. Lee,[41] S. H. Lee,[41] Y.-J. Lee,[29] T. Lesiak,[30] J. Li,[40] A. Limosani,[23] S.-W. Lin,[29] D. Liventsev,[14] J. MacNaughton,[13] G. Majumder,[44] F. Mandl,[13] D. Marlow,[37] T. Matsuishi,[24] H. Matsumoto,[32] S. Matsumoto,[5] T. Matsumoto,[50] A. Matyja,[30] Y. Mikami,[47] W. Mitaroff,[13] K. Miyabayashi,[25] Y. Miyabayashi,[24] H. Miyake,[34] H. Miyata,[32] R. Mizuk,[14] D. Mohapatra,[55] G. R. Moloney,[23] G. F. Moorhead,[23] T. Mori,[49] A. Murakami,[39] T. Nagamine,[47] Y. Nagasaka,[11] T. Nakadaira,[48] I. Nakamura,[10] E. Nakano,[33] M. Nakao,[10] H. Nakazawa,[10] Z. Natkaniec,[30] K. Neichi,[46] S. Nishida,[10] O. Nitoh,[51] S. Noguchi,[25] T. Nozaki,[10] A. Ogawa,[38] S. Ogawa,[45] T. Ohshima,[24] T. Okabe,[24] S. Okuno,[16] S. L. Olsen,[9] Y. Onuki,[32] W. Ostrowicz,[30] H. Ozaki,[10] P. Pakhlov,[14] H. Palka,[30] C. W. Park,[42] H. Park,[19] K. S. Park,[42] N. Parslow,[43] L. S. Peak,[43] M. Pernicka,[13] J.-P. Perroud,[20] M. Peters,[9] L. E. Piilonen,[55] A. Poluektov,[2] F. J. Ronga,[10] N. Root,[2] M. Rozanska,[30] H. Sagawa,[10] M. Saigo,[47] S. Saitoh,[10] Y. Sakai,[10] H. Sakamoto,[18] T. R. Sarangi,[10] M. Satapathy,[54] N. Sato,[24] O. Schneider,[20] J. Schümann,[29] C. Schwanda,[13] A. J. Schwartz,[6] T. Seki,[50] S. Semenov,[14] K. Senyo,[24] Y. Settai,[5] R. Seuster,[9] M. E. Sevior,[23] T. Shibata,[32] H. Shibuya,[45] B. Shwartz,[2] V. Sidorov,[2] V. Siegle,[38] J. B. Singh,[35] A. Somov,[6] N. Soni,[35] R. Stamen,[10] S. Stanič,[53,*] M. Starič,[15] A. Sugi,[24] A. Sugiyama,[39] K. Sumisawa,[34] T. Sumiyoshi,[50] S. Suzuki,[39] S. Y. Suzuki,[10] O. Tajima,[10]

F. Takasaki,[10] K. Tamai,[10] N. Tamura,[32] K. Tanabe,[48] M. Tanaka,[10] G. N. Taylor,[23] Y. Teramoto,[33] X. C. Tian,[36] S. Tokuda,[24] S. N. Tovey,[23] K. Trabelsi,[9] T. Tsuboyama,[10] T. Tsukamoto,[10] K. Uchida,[9] S. Uehara,[10] T. Uglov,[14] K. Ueno,[29] Y. Unno,[3] S. Uno,[10] Y. Ushiroda,[10] G. Varner,[9] K. E. Varvell,[43] S. Villa,[20] C. C. Wang,[29] C. H. Wang,[28] J. G. Wang,[55] M.-Z. Wang,[29] M. Watanabe,[32] Y. Watanabe,[49] L. Widhalm,[13] Q. L. Xie,[12] B. D. Yabsley,[55] A. Yamaguchi,[47] H. Yamamoto,[47] S. Yamamoto,[50] T. Yamanaka,[34] Y. Yamashita,[31] M. Yamauchi,[10] Heyoung Yang,[41] P. Yeh,[29] J. Ying,[36] K. Yoshida,[24] Y. Yuan,[12] Y. Yusa,[47] H. Yuta,[1] S. L. Zang,[12] C. C. Zhang,[12] J. Zhang,[10] L. M. Zhang,[40] Z. P. Zhang,[40] V. Zhilich,[2] T. Ziegler,[37] D. Žontar,[21,15] and D. Zürcher[20]

(The Belle Collaboration)

[1]*Aomori University, Aomori*
[2]*Budker Institute of Nuclear Physics, Novosibirsk*
[3]*Chiba University, Chiba*
[4]*Chonnam National University, Kwangju*
[5]*Chuo University, Tokyo*
[6]*University of Cincinnati, Cincinnati, Ohio 45221*
[7]*University of Frankfurt, Frankfurt*
[8]*Gyeongsang National University, Chinju*
[9]*University of Hawaii, Honolulu, Hawaii 96822*
[10]*High Energy Accelerator Research Organization (KEK), Tsukuba*
[11]*Hiroshima Institute of Technology, Hiroshima*
[12]*Institute of High Energy Physics, Chinese Academy of Sciences, Beijing*
[13]*Institute of High Energy Physics, Vienna*
[14]*Institute for Theoretical and Experimental Physics, Moscow*
[15]*J. Stefan Institute, Ljubljana*
[16]*Kanagawa University, Yokohama*
[17]*Korea University, Seoul*
[18]*Kyoto University, Kyoto*
[19]*Kyungpook National University, Taegu*
[20]*Swiss Federal Institute of Technology of Lausanne, EPFL, Lausanne*
[21]*University of Ljubljana, Ljubljana*
[22]*University of Maribor, Maribor*
[23]*University of Melbourne, Victoria*
[24]*Nagoya University, Nagoya*
[25]*Nara Women's University, Nara*
[26]*National Central University, Chung-li*
[27]*National Kaohsiung Normal University, Kaohsiung*
[28]*National United University, Miao Li*
[29]*Department of Physics, National Taiwan University, Taipei*
[30]*H. Niewodniczanski Institute of Nuclear Physics, Krakow*
[31]*Nihon Dental College, Niigata*
[32]*Niigata University, Niigata*
[33]*Osaka City University, Osaka*
[34]*Osaka University, Osaka*
[35]*Panjab University, Chandigarh*

[36]*Peking University, Beijing*
[37]*Princeton University, Princeton, New Jersey 08545*
[38]*RIKEN BNL Research Center, Upton, New York 11973*
[39]*Saga University, Saga*
[40]*University of Science and Technology of China, Hefei*
[41]*Seoul National University, Seoul*
[42]*Sungkyunkwan University, Suwon*
[43]*University of Sydney, Sydney NSW*
[44]*Tata Institute of Fundamental Research, Bombay*
[45]*Toho University, Funabashi*
[46]*Tohoku Gakuin University, Tagajo*
[47]*Tohoku University, Sendai*
[48]*Department of Physics, University of Tokyo, Tokyo*
[49]*Tokyo Institute of Technology, Tokyo*
[50]*Tokyo Metropolitan University, Tokyo*
[51]*Tokyo University of Agriculture and Technology, Tokyo*
[52]*Toyama National College of Maritime Technology, Toyama*
[53]*University of Tsukuba, Tsukuba*
[54]*Utkal University, Bhubaneswer*
[55]*Virginia Polytechnic Institute and State University, Blacksburg, Virginia 24061*
[56]*Yonsei University, Seoul*

Abstract

We report measurements of the differential q^2 spectrum and the forward-backward asymmetry for $B \to K^{(*)}\ell^+\ell^-$, where ℓ represents an electron or a muon, with a data sample of 253 fb^{-1} accumulated on the $\Upsilon(4S)$ resonance with the Belle detector at KEKB. We also present measurements of the branching fractions and their ratios.

PACS numbers: 13.20.He, 11.30.Hv

Flavor-changing neutral current (FCNC) processes are forbidden at tree level in the Standard Model (SM); rather, they proceed at a low rate via loop or box diagrams. If additional like diagrams with non-SM particles contribute to such a decay, their amplitudes will interfere with the SM amplitudes and thereby modify the decay rate as well as other properties. This feature makes FCNC processes an ideal place to search for new physics.

Measurements of the radiative penguin decay $B \to X_s\gamma$ [1, 2, 3], which are consistent with the SM prediction, strongly constrain the magnitude—but not the sign—of the effective Wilson coefficient C_7. This is an important limitation, since non-SM contributions can change the sign of C_7 without changing the $B \to X_s\gamma$ branching fraction [4].

The $b \to s\ell^+\ell^-$ process is promising from this point of view, since not only the photonic penguin diagram but also the Z-penguin and box diagrams contribute to this decay mode. As a result, the Wilson coefficients C_7, C_9 and C_{10} can be completely determined. The first observations of $B \to K\ell^+\ell^-$, $B \to K^*\ell^+\ell^-$ and inclusive $B \to X_s\ell^+\ell^-$ decays were reported by the Belle Collaboration [5, 6, 7]. The measured branching fractions of these decay modes were used to exclude a large area of the allowed region in the C_9-C_{10} plane [8, 9]. However, the determination of the sign of C_7 (as well as of C_9 and C_{10}) requires precise measurements of the distribution in squared dilepton momentum q^2 and the forward-backward asymmetry in these decay modes [10].

In this paper, we present preliminary results of improved measurements of $B \to K\ell^+\ell^-$ and $B \to K^*\ell^+\ell^-$ using data produced in e^+e^- annihilation at the KEKB asymmetric collider [11] and collected with the Belle detector. The data sample corresponds to 253 fb^{-1} taken at the $\Upsilon(4S)$ resonance and contains approximately 275 million $B\overline{B}$ pairs.

The Belle detector is a large-solid-angle magnetic spectrometer that consists of a silicon vertex detector (SVD), a 50-layer central drift chamber (CDC), an array of aerogel threshold Čerenkov counters (ACC), a barrel-like arrangement of time-of-flight scintillation counters (TOF), and an electromagnetic calorimeter (ECL) comprised of CsI(Tl) crystals located inside a super-conducting solenoid coil that provides a 1.5 T magnetic field. An iron flux-return located outside of the coil is instrumented to detect K_L^0 mesons and to identify muons (KLM). The detector is described in detail elsewhere [12]. The data were collected with two different inner detector configurations. For the first sample of 152 million $B\bar{B}$ pairs, a 2.0 cm radius beampipe and a 3-layer silicon vertex detector were used; for the latter 123 million $B\bar{B}$ pairs, a 1.5 cm radius beampipe, a 4-layer silicon detector, and a small-cell inner drift chamber were used [13].

In this analysis, primary charged tracks—except for the daughters from $K_S \to \pi^+\pi^-$ decays—are required to have impact parameters relative to the interaction point of less than 5.0 cm along the z axis (aligned opposite the positron beam) and less than 0.5 cm in the $r\phi$ plane that is transverse to this axis. This requirement reduces the combinatorial background from photon conversion, beam-gas and beam-wall events.

Charged tracks are identified as either kaons or pions by a likelihood ratio based on the CDC specific ionization, time-of-flight information and the light yield in the ACC. This classification is superseded for a track that is identified as an electron or for a pion-like track that is identified as a muon. Electrons are identified from the ratio of shower energy of the matching ECL cluster to the momentum measured by the CDC, the transverse shower shape of this cluster, the specific ionization in the CDC and the ACC response. We require that the electron momentum be greater than 0.4 GeV/c to reach the ECL. Muons are identified by their penetration depth and transverse scattering in the KLM. The muon momentum is required to exceed 0.7 GeV/c. The muon identification criteria are more stringent for

momenta below 1.0 GeV/c to suppress misidentified hadrons.

Photons are selected from isolated neutral clusters in the ECL with energy greater than 50 MeV and a shape that is consistent with an electromagnetic shower. Neutral pion candidates are reconstructed from pairs of photons, and are required to have an invariant mass within 10 MeV/c^2 of the nominal π^0 mass and a laboratory momentum greater than 0.1 GeV/c. The pion momentum is recalculated by constraining the invariant mass to the nominal π^0 mass. K^0_S candidates are reconstructed from oppositely charged pions that have invariant masses within 15 MeV/c^2 of the nominal K^0_S mass. We impose additional criteria based on the radial impact parameters of the pions (δr), the distance between the closest approaches of the pions along the beam direction (δz), the distance of the vertex from the interaction point (l), and the azimuthal angle difference between the vertex direction and the K^0_S momentum direction ($\delta\phi$). These variables are combined as follows: for $p_{K^0_S} < 0.5$ GeV/c, $\delta z < 8$ mm, $\delta r > 0.5$ mm, and $\delta\phi < 0.3$ rad are required; for 0.5 GeV/$c < p_{K^0_S} < 1.5$ GeV/c, $\delta z < 18$ mm, $\delta r > 0.3$ mm, $\delta\phi < 0.1$ rad, and $l > 0.8$ mm are required; and for $p_{K^0_S} > 1.5$ GeV/c, $\delta z < 24$ mm, $\delta r > 0.2$ mm, $\delta\phi < 0.03$ rad, and $l > 2.2$ mm are required.

K^* candidates are formed by combining a kaon and a pion: $K^+\pi^-$, $K^0_S\pi^+$ or $K^+\pi^0$ [14]. The K^* invariant mass is required to lie within 75 MeV/c^2 of the nominal K^* mass. For modes involving neutral pions, combinatorial backgrounds are reduced by the additional requirement $\cos\theta_{\rm hel} < 0.8$, where $\theta_{\rm hel}$ is defined as the angle between the opposite of B momentum and the kaon momentum direction in the K^* rest frame.

B candidates are reconstructed from a $K^{(*)}$ candidate and an oppositely-charged lepton pair. We use two variables defined in the CM frame to select B candidates: the beam-energy constrained mass $M_{\rm bc} = \sqrt{{E^*_{\rm beam}}^2 - {p^*_B}^2}$ and the energy difference $\Delta E = E^*_B - E^*_{\rm beam}$, where p^*_B and E^*_B are the measured momentum and energy, respectively, of the B candidate, and $E^*_{\rm beam}$ is the beam energy [15]. When multiple candidates are found in an event, we select the candidate with the smallest value of $|\Delta E|$.

Backgrounds from $B \to J/\psi(\psi')K^{(*)}$ are rejected using the dilepton invariant mass. The veto windows are defined as

-0.25 GeV/$c^2 < M_{e^+e^-} - M_{J/\psi} < 0.07$ GeV/c^2	for K^* modes
-0.20 GeV/$c^2 < M_{e^+e^-} - M_{J/\psi} < 0.07$ GeV/c^2	for K modes
-0.20 GeV/$c^2 < M_{e^+e^-} - M_{\psi'} < 0.07$ GeV/c^2	for K^* and K modes
-0.15 GeV/$c^2 < M_{\mu^+\mu^-} - M_{J/\psi} < 0.08$ GeV/c^2	for K^* modes
-0.10 GeV/$c^2 < M_{\mu^+\mu^-} - M_{J/\psi} < 0.08$ GeV/c^2	for K modes
-0.10 GeV/$c^2 < M_{\mu^+\mu^-} - M_{\psi'} < 0.08$ GeV/c^2	for K^* and K modes

If a photon with energy less than 500 MeV is found in the 50 mrad cone along the electron momentum direction, we reapply the above vetoes with the invariant mass calculated including this photon to reject the background with a bremsstrahlung photon, $J/\psi(\psi') \to e^+e^-\gamma(\gamma)$. For $K^*e^+e^-$ modes, $B \to J/\psi\, K$ can be a background if a bremsstrahlung photon is missed and a pion from the other B meson in the event is included. We suppress this background by the following prescription: the included pion is discarded and an unobserved bremsstrahlung photon is added with a direction parallel to the electron or positron and an energy that gives $\Delta E = 0$ for the B candidate. If the dilepton mass and the beam-energy constrained mass are consistent with a $B \to J/\psi\, K$ event, the candidate is vetoed.

We suppress background from photon conversions and π^0 Dalitz decays by requiring the dielectron mass to satisfy $M_{e^+e^-} > 0.14$ GeV/c^2. This cut eliminates possible peaking background from $B \to K^*\gamma$ and $B \to K^{(*)}\pi^0$.

Background from continuum $q\overline{q}$ events is suppressed using event topology. Continuum events have a jet-like shape while $B\overline{B}$ events have a spherical shape in the center-of-mass frame. A Fisher discriminant $\mathcal{F}$ [16] is calculated from the energy flow in 9 cones along the B candidate sphericity axis and the normalized second Fox-Wolfram moment R_2 [17]. We combine this with the cosine of the polar angle $\cos\theta_B^*$ of the B meson flight direction and the cosine of the polar angle $\cos\theta_{\rm sph}^*$ of the B meson sphericity axis to define likelihoods $\mathcal{L}_{\rm sig}$ and $\mathcal{L}_{\rm cont}$ for signal and continuum background, respectively, and then cut on the likelihood ratio $\mathcal{R}_{\rm cont} = \mathcal{L}_{\rm sig}/(\mathcal{L}_{\rm sig} + \mathcal{L}_{\rm cont})$. For the muon mode, $|\cos\theta_{\rm sph}^*|$ is not used since its distribution is nearly the same for signal and continuum within the detector acceptance.

The dominant background from $B\overline{B}$ events is due to semileptonic B decays. The missing energy of the event, $E_{\rm miss} = 2E_{\rm beam}^* - E_{\rm vis}^*$ where $E_{\rm vis}^*$ is a total visible energy in the event, is used to suppress this background since the undetected neutrinos carry away a substantial amount of energy. The B meson flight angle, $\cos\theta_B^*$, is also used to suppress combinatorial background in $B\overline{B}$ events. We combine $E_{\rm miss}$ and $\cos\theta_B^*$ into signal and $B\overline{B}$-background likelihoods and cut on the likelihood ratio $\mathcal{R}_{B\overline{B}}$, defined similarly to $\mathcal{R}_{\rm cont}$.

The $B \to K^{(*)}\ell^+\ell^-$ decays are generated according to Ref [8] and then processed by a GEANT-based Monte Carlo (MC) simulation to estimate the efficiencies. The signal box is defined as $|M_{\rm bc} - M_B| < 0.007$ GeV/c^2 for both lepton modes and -0.055 GeV$< \Delta E <$ 0.035 GeV ($|\Delta E| < 0.035$ GeV) for the electron (muon) mode. We make distinct selections on $\mathcal{R}_{\rm cont}$ and $\mathcal{R}_{B\overline{B}}$ for each decay mode. The detection efficiencies are estimated from the MC samples and are summarized in Table I.

To determine the signal yield, we perform a binned maximum-likelihood fit to each $M_{\rm bc}$ distribution. The expected number of signal events is calculated as a function of $M_{\rm bc}$ using a Gaussian signal distribution plus background functions. The mean and the width of the signal Gaussian are determined using observed $J/\psi K^{(*)}$ events. A MC study shows that the width has no dependence on the dilepton invariant mass. We consider backgrounds from three sources: semileptonic decays, decays containing J/ψ and ψ' mesons, and double misidentification of hadrons as leptons. The background from semileptonic decays is parameterized by the ARGUS function [20]. The shape is determined from large $B\bar{B}$ and continuum MC samples, each containing at least one oppositely charged lepton pair. The shape parameter obtained from MC is consistent with that taken from a data sample of $B \to K^{(*)}e^\pm\mu^\mp$ candidates. The residual background from J/ψ and ψ' mesons that cannot be removed by the $\psi^{(\prime)}$ veto windows is estimated from a large MC sample of J/ψ and ψ' inclusive events and parameterized by an ARGUS function and a Gaussian. The background contribution due to misidentification of hadrons as leptons is parameterized by another ARGUS function and a Gaussian. The ARGUS function represents the combinatorial background while the Gaussian represents the component that forms a peak in the $M_{\rm bc}$ distribution. The shape and normalization of this background are fixed using the $B \to K^{(*)}h^+h^-$ data sample (where h refers to a pion or kaon). All $K^{(*)}h^+h^-$ combinations are weighted by the momentum- and polar angle-dependent probability of misidentifying $K^{(*)}h^+h^-$ as $K^{(*)}\ell^+\ell^-$. This study yields 1.06 ± 0.09 Kh^+h^- events and 0.60 ± 0.05 $K^*h^+h^-$ events in the peak region. Other backgrounds with misidentified leptons are negligible. The normalizations of the signal and the background from real leptons are floated in the fit. The fit results are shown in Fig. 1 and Table I.

We observe $78.5^{+10.7}_{-10.0}$ $B \to K^*\ell^+\ell^-$ signal with a significance of 11.0 and $82.2^{+11.4}_{-10.7}$ $B \to K\ell^+\ell^-$ signal with a significance of 10.1. The significance is defined as $\sqrt{-2\ln(\mathcal{L}_0/\mathcal{L}_{\rm max})}$, where $\mathcal{L}_{\rm max}$ is the maximum likelihood in the $M_{\rm bc}$ fit and $\mathcal{L}_0$ is the likelihood of the best

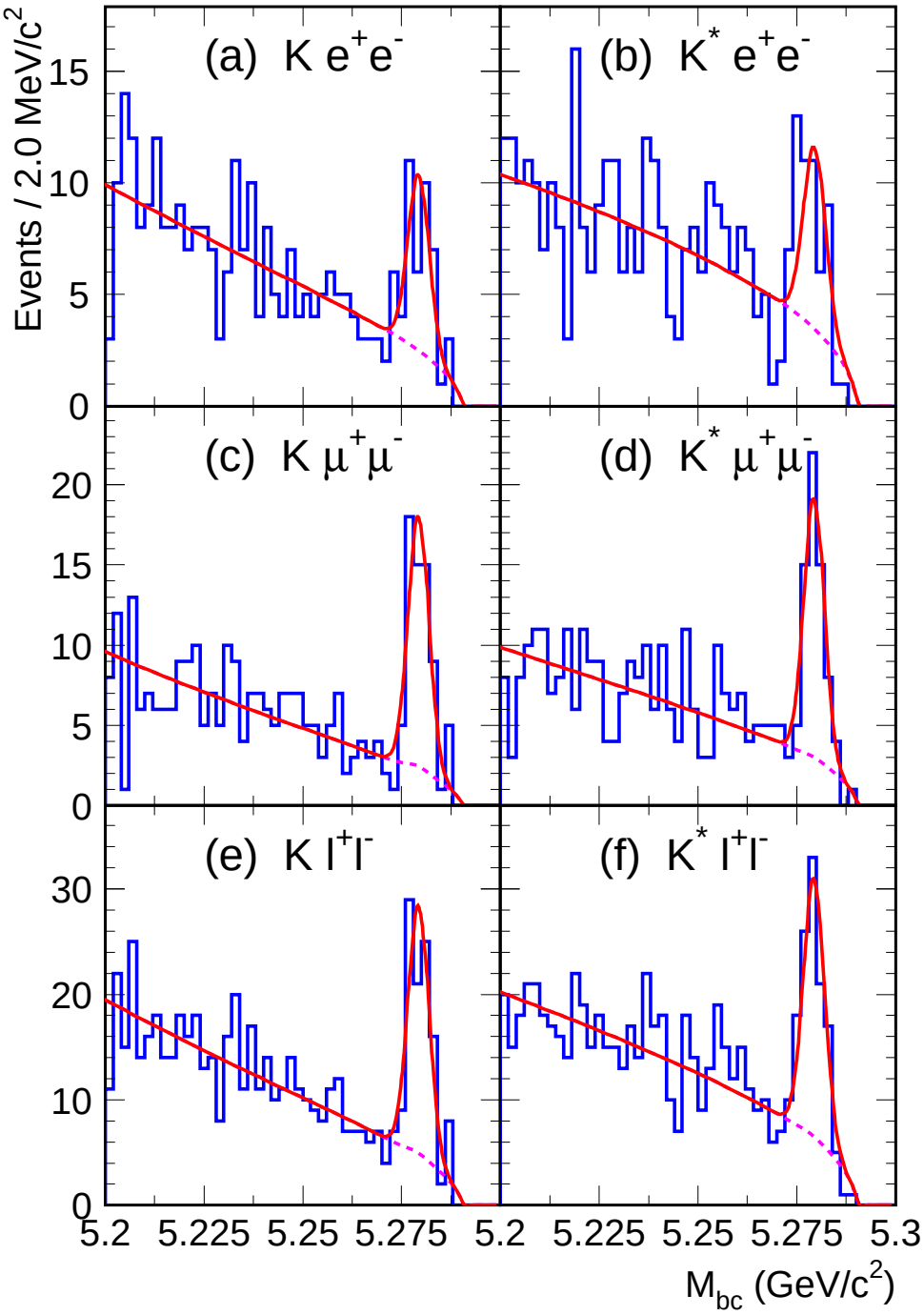

FIG. 1: $M_{\rm bc}$ distributions for (a) $B \to Ke^+e^-$, (b) $B \to K^*e^+e^-$, (c) $B \to K\mu^+\mu^-$, (d) $B \to K^*\mu^+\mu^-$, (e) $B \to K\ell^+\ell^-$ and (f) $B \to K^*\ell^+\ell^-$ samples. The solid and dashed curves are the fit results of the total and background contributions.

fit when the signal yield is constrained to be zero. Since the signal and background shapes are fixed in the fitting, the error due to uncertainty in shape parameters is included in the systematic error. We determine this by varying each shape parameter by $\pm 1\sigma$ and recalculating the signal yield. We quote the smallest resulting significance in our determinations above.

TABLE I: Summary of the fit results and branching fractions. Signal yield estimated from the $M_{\rm bc}$ fit, detection efficiency for each mode, obtained branching fraction, 90% confidence level upper limit of the branching fraction and the significance of the signal. The first error in the signal yield and branching fraction is statistical, the second is systematic and the third is due to model dependence. The first error in the efficiency is due to MC statistics and systematic effects and the second one is due to model dependence.

Mode	Signal yield	Efficiency [%]	$\mathcal{B}$ [$\times 10^{-7}$]	U.L.[$\times 10^{-7}$]	Signif.
$K^0e^+e^-$	$-1.0^{+1.8+0.2}_{-1.2-0.4}$	$5.10 \pm 0.29 \pm 0.20$	$-0.70^{+1.29+0.14}_{-0.82-0.28} \pm 0.03$	3.0	0.0
$K^+e^+e^-$	$28.6^{+6.7+0.5}_{-6.0-0.7}$	$16.3 \pm 0.7 \pm 0.1$	$6.40^{+1.50+0.29}_{-1.34-0.31} \pm 0.05$	-	6.4
Ke^+e^-	$26.6^{+6.8+0.6}_{-6.1-0.8}$	$10.7 \pm 0.5 \pm 0.1$	$4.54^{+1.16+0.22}_{-1.04-0.24} \pm 0.06$	-	5.5
$K^{*0}e^+e^-$	$22.0^{+6.6+0.9}_{-5.9-0.7}$	$4.32 \pm 0.22 \pm 0.36$	$18.5^{+5.5}_{-4.9} \pm 1.1 \pm 1.5$	-	4.4
$K^{*+}e^+e^-$	$6.2^{+4.1+0.3}_{-3.4-0.6}$	$1.42 \pm 0.08 \pm 0.06$	$16.0^{+10.4+1.2}_{-8.7\ -1.8} \pm 0.7$	37	1.7
$K^*e^+e^-$	$28.9^{+7.6}_{-6.9} \pm 0.9$	$2.87 \pm 0.15 \pm 0.21$	$18.4^{+4.8}_{-4.4} \pm 1.1 \pm 1.3$	-	4.8
$K^0\mu^+\mu^-$	$11.6^{+4.0+0.1}_{-3.4-0.3}$	$6.76 \pm 0.41 \pm 0.04$	$6.26^{+2.17+0.38}_{-1.81-0.41} \pm 0.04$	-	5.1
$K^+\mu^+\mu^-$	$39.9^{+7.6+0.5}_{-6.9-0.7}$	$23.2 \pm 1.1 \pm 0.5$	$6.28^{+1.19+0.30}_{-1.08-0.31} \pm 0.13$	-	8.3
$K\mu^+\mu^-$	$51.5^{+8.4+0.5}_{-7.8-0.7}$	$15.0 \pm 0.7 \pm 0.2$	$6.26^{+1.03+0.31}_{-0.64-0.32} \pm 0.10$	-	9.7
$K^{*0}\mu^+\mu^-$	$40.7^{+7.6+0.5}_{-6.9-0.6}$	$8.01 \pm 0.43 \pm 0.14$	$18.5^{+3.5}_{-3.1} \pm 1.0 \pm 0.3$	-	8.4
$K^{*+}\mu^+\mu^-$	$11.4^{+4.5+0.2}_{-3.8-0.6}$	$2.55 \pm 0.14 \pm 0.08$	$16.3^{+6.4+0.9}_{-5.4-1.2} \pm 0.5$	-	3.5
$K^*\mu^+\mu^-$	$52.5^{+8.7+0.5}_{-8.0-0.8}$	$5.28 \pm 0.29 \pm 0.03$	$18.1^{+3.0}_{-2.8} \pm 1.1 \pm 0.1$	-	9.1
$K^0\ell^+\ell^-$	$10.7^{+4.4+0.2}_{-3.7-0.5}$	$5.95 \pm 0.36 \pm 0.11$	$3.28^{+1.34+0.21}_{-1.13-0.25} \pm 0.06$	-	3.5
$K^+\ell^+\ell^-$	$68.6^{+9.9+0.8}_{-9.3-1.0}$	$19.8 \pm 0.9 \pm 0.2$	$6.32^{+0.92}_{-0.85} \pm 0.29 \pm 0.06$	-	9.4
$K\ell^+\ell^-$	$78.5^{+10.7+0.8}_{-10.0-1.1}$	$13.0 \pm 0.6 \pm 0.4$	$5.50^{+0.75}_{-0.70} \pm 0.27 \pm 0.02$	-	11.0
$K^{*0}\ell^+\ell^-$	$63.8^{+9.9}_{-9.2} \pm 0.9$	$6.88 \pm 0.37 \pm 0.30$	$16.9^{+2.6}_{-2.4} \pm 0.9 \pm 0.7$	-	9.4
$K^{*+}\ell^+\ell^-$	$16.3^{+5.6+0.5}_{-4.9-0.8}$	$2.22 \pm 0.13 \pm 0.02$	$13.4^{+4.6+0.9}_{-4.0-1.0} \pm 0.1$	-	3.7
$K^*\ell^+\ell^-$	$82.2^{+11.4+1.0}_{-10.7-1.1}$	$4.55 \pm 0.24 \pm 0.12$	$16.5^{+2.3}_{-2.2} \pm 0.9 \pm 0.4$	-	10.1

We consider experimental systematic effects from the fit, the efficiency determination and $B\overline{B}$ event counting. Uncertainty in the background function is the dominant source of the systematic error. To evaluate the change caused by the uncertainty in the signal function parameters, the mean and the width of the Gaussian are changed by $\pm 1\sigma$ from the values determined from $J/\psi K^{(*)}$ events. The uncertainty in the background shape is obtained by varying the ARGUS shape parameter by $\pm 1\sigma$ from the value determined with a large MC sample. The uncertainty in the peaking background contribution is evaluated by changing the area of the associated Gaussian by $\pm 1\sigma$. The systematic errors associated with the fit function are shown in the second column of Table I. Systematic uncertainties in the tracking, charged kaon identification, charged pion identification, electron identification,

muon identification, K^0_S detection and π^0 detection efficiencies are estimated to be 1.0%, 1.0%, 0.8%, 0.5%, 1.2%, 4.5% and 2.7% per particle, respectively. The uncertainty in the background suppression is estimated to be 2.3% using $J/\psi K^{(*)}$ control samples. The systematic error due to MC statistics is less than 0.7%. The uncertainty in $B\overline{B}$ event counting is 1.1%. The systematic errors associated with efficiency and $B\overline{B}$ event counting are summarized in Table II. Total experimental systematic errors are calculated by adding all systematic errors in quadrature.

The systematic uncertainty due to theoretical modeling is also evaluated. We apply the same selection criteria on the signal samples generated according to the three form factor models [8, 18, 19] and obtain the efficiencies. The maximum difference in these efficiencies is assigned as uncertainty in model dependence and is listed as the final value in column four of Table I.

Source	K^0	K^+	$K^+\pi^-$	$K^0_S\pi^+$	$K^+\pi^0$
Tracking	2.0	3.0	4.0	3.0	3.0
Kaon identification	-	1.0	1.0	-	1.0
Pion identification	-	-	0.8	0.8	-
Lepton identification (e/μ)	1.0/2.4	1.0/2.4	1.0/2.4	1.0/2.4	1.0/2.4
K^0_S detection	4.5	-	-	4.5	-
π^0 detection	-	-	-	-	2.7
BG suppression	2.3	2.3	2.3	2.3	2.3
$B\overline{B}$ event counting	1.1	1.1	1.1	1.1	1.1
total (e/μ)	5.8/6.1	4.2/4.7	5.1/5.5	6.7/6.8	6.3/6.1

TABLE II: Summary of systematic errors in efficiencies and $B\overline{B}$ event counting.

In the calculation of the branching fraction, we assume equal production rates of charged and neutral B meson pairs from $\Upsilon(4S)$ as well as isospin invariance. When combining the $K^*e^+e^-$ and $K^*\mu^+\mu^-$ modes, we assume the ratio of branching fraction of $K^*\mu^+\mu^-$ to that of $K^*e^+e^-$ to be 0.75 [8]. The combined branching fraction corresponds to the muon mode. The branching fractions are found to be

$$\mathcal{B}(B \to K\ell^+\ell^-) = (5.50^{+0.75}_{-0.70} \pm 0.27 \pm 0.02) \times 10^{-7}$$
$$\mathcal{B}(B \to K^*\ell^+\ell^-) = (16.5^{+2.3}_{-2.2} \pm 0.9 \pm 0.4) \times 10^{-7},$$

where the first error is statistical, the second is systematic, and the third is due to model dependence. These values are consistent with the SM predictions [8, 18, 19, 21]. The branching fraction of $B \to K^*\ell^+\ell^-$ is slightly larger than our previous result [6]. Since we now use NNLO effective Wilson coefficients [8], which gives larger C_7 and smaller C_9 values than the older NLO calculation, the efficiency of $B \to K^*\ell^+\ell^-$ is smaller by about 12%. As a result, the branching fraction is now higher. (With the NLO effective Wilson coefficients, the branching fraction becomes 14.7×10^{-7}, which is consistent with our previous result.) The branching fractions of the other decay modes are listed in Table I.

For the modes with a significance of less than 3.0, we also set 90% confidence level (C.L.) upper limits for the branching fractions. The 90% C.L. upper limit yield N is defined as $\int_0^N \mathcal{L}(n)dn = 0.9 \int_0^\infty \mathcal{L}(n)dn$. The function $\mathcal{L}(n)$ is the likelihood with signal yield n, where

each signal and background shape parameter is modified up or down by its systematic error in the direction that increases the signal yield. The upper limits for the branching fraction are then calculated by reducing the efficiency by its systematic error.

We calculate the ratios of branching fractions to muon and electron modes. The ratio of branching fraction of $B \to K\mu^+\mu^-$ to $B \to Ke^+e^-$ ($\mathcal{R}_{K\ell\ell}$)is sensitive to neutral Higgs emission from the internal loop in the two Higgs doublet model with large $\tan\beta$ [22]. If the Higgs contribution is sizable, this ratio is greater than unity. The corresponding ratio for $B \to K^*\ell^+\ell^-$ ($\mathcal{R}_{K^*\ell\ell}$) is sensitive to the size of photon pole and is predicted to be about 0.75 in the SM. The ratios are measured to be

$$\mathcal{R}_{K\ell\ell} = 1.38^{+0.39+0.06}_{-0.41-0.07}$$
$$\mathcal{R}_{K^*\ell\ell} = 0.98^{+0.30}_{-0.31} \pm 0.08,$$

which are consistent with the SM predictions.

The distribution of the squared dilepton momenum q^2 and forward-backward asymmetries in $B \to K\ell^+\ell^-$ and $K^*\ell^+\ell^-$ are also measured. The forward-backward asymmetry ($A_{\rm FB}$) is defined as the partial rate asymmetry between the positive and negative regions of $\cos\theta_{B\ell^+}$, the cosine of the angle between the B^0 or B^+ meson and positive charged lepton momentum directions in the dilepton rest frame,

$$A_{\rm FB} = \frac{\Gamma(\cos\theta_{B\ell^+} > 0) - \Gamma(\cos\theta_{B\ell^+} < 0)}{\Gamma(\cos\theta_{B\ell^+} > 0) + \Gamma(\cos\theta_{B\ell^+} < 0)}.$$

The signal yield is extracted from a fit to the $M_{\rm bc}$ distributions in each q^2 bin and $\cos\theta_{B\ell^+}$ region. This procedure takes into account the forward-backward asymmetry of the background. The q^2 resolution is about 0.6% and this is small enough relative to the bin size. For the q^2 distribution measurement, the efficiency in each q^2 bin is obtained from the MC samples described earlier. The branching fraction at low q^2 differs between $K^*e^+e^-$ and $K^*\mu^+\mu^-$; we use the average in calculating the $K^*\ell^+\ell^-$ differential branching fraction. Figure 2 and Table III show the q^2 distributions; they are in agreement with the SM predictions.

Figure 3 shows the raw forward-backward asymmetry distributions for $B \to K\ell^+\ell^-$ and $K^*\ell^+\ell^-$. The asymmetry in $B \to K\ell^+\ell^-$ is expected to vanish in the SM; this expectation is essentially unchanged by the presence of new physics [23]. Therefore, $B \to K\ell^+\ell^-$ is a good control sample for the more interesting forward-backward asymmetry in $B \to K^*\ell^+\ell^-$. The measured asymmetry for $B \to K\ell^+\ell^-$ is indeed consistent with zero. For $B \to K^*\ell^+\ell^-$, the asymmetry is in agreement with both the SM and the wrong-sign C_7 expectations, since the statistical power is not yet sufficient to distinguish between these two cases.

In summary, we report first measurement of forward-backward asymmetry as a function of q^2 in $B \to K^*\ell^+\ell^-$. Within the limited statistical precision, the measured asymmetry in $B \to K^*\ell^+\ell^-$ is consistent with both the SM and the wrong sign C_7 case. We also report improved measurements of the branching fractions of $B \to K\ell^+\ell^-$ and $B \to K^*\ell^+\ell^-$. The measured values, their ratios and the q^2 distributions for $B \to K\ell^+\ell^-$ and $B \to K^*\ell^+\ell^-$ are in good agreement with the SM predictions [8, 18, 19, 21].

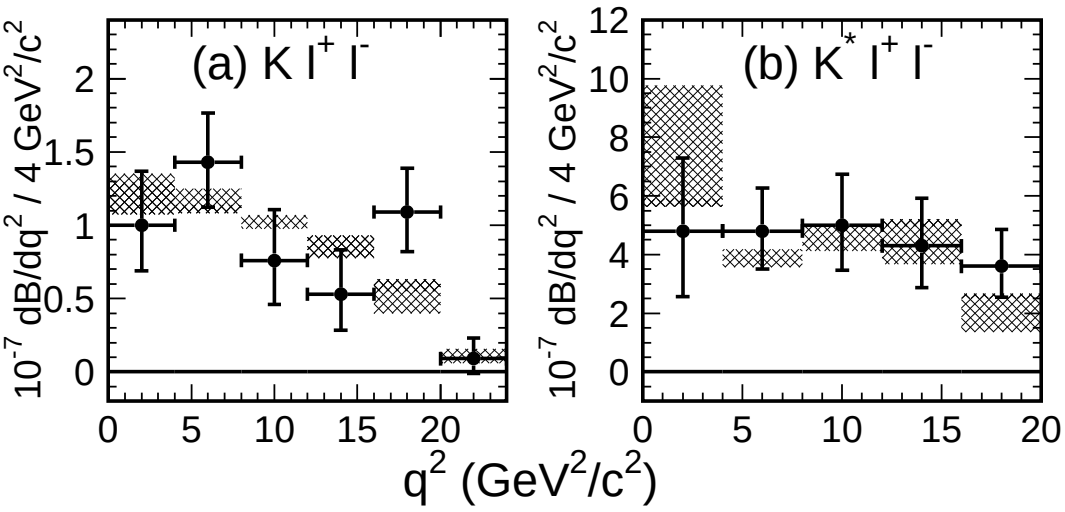

FIG. 2: The q^2 distributions of (a) $K\ell^+\ell^-$ and (b) $K^*\ell^+\ell^-$. Points with error bars show the data, while the hatched bands show the range of the SM predictions [8, 18, 19].

$K\ell^+\ell^-$			
q^2/GeV^2	yield	efficiency[%]	B[$\times 10^{-7}$]
$[0,4]$	$12.4\,^{+4.4\,+0.3}_{-3.7\,-0.4}$	$11.3 \pm 0.5 \pm 0.1$	$1.00\,^{+0.36}_{-0.30} \pm 0.06 \pm 0.01$
$[4,8]$	$26.7\,^{+6.1}_{-5.4} \pm 0.4$	$17.0 \pm 0.8 \pm 0.3$	$1.43\,^{+0.32}_{-0.29} \pm 0.07 \pm 0.01$
$[8,12]$	$10.1\,^{+4.5\,+0.4}_{-3.8\,-0.5}$	$12.0 \pm 0.6 \pm 0.1$	$0.76\,^{+0.34\,+0.05}_{-0.29\,-0.06} \pm 0.01$
$[12,16]$	$6.5\,^{+3.6}_{-2.9} \pm 0.3$	$11.1 \pm 0.5 \pm 0.3$	$0.53\,^{+0.30}_{-0.24} \pm 0.04 \pm 0.01$
$[16,20]$	$20.4\,^{+5.4\,+0.4}_{-4.8\,-0.5}$	$17.0 \pm 0.8 \pm 0.3$	$1.09\,^{+0.29\,+0.05}_{-0.26\,-0.06} \pm 0.02$
$[20,24]$	$1.3\,^{+2.1}_{-1.4} \pm 0.3$	$13.2 \pm 0.6 \pm 0.8$	$0.09\,^{+0.14}_{-0.10} \pm 0.02 \pm 0.006$
$K^*\ell^+\ell^-$			
q^2 GeV^2	yield	efficiency[%]	B[$\times 10^{-7}$]
$[0,4]$	$11.3\,^{+4.9}_{-4.2} \pm 0.6$	$2.16 \pm 0.11 \pm 0.56$	$4.8\,^{+2.1}_{-1.8} \pm 0.4 \pm 1.2$
$[4,8]$	$21.6\,^{+6.1\,+0.4}_{-5.4\,-0.6}$	$4.09 \pm 0.22 \pm 0.11$	$4.8\,^{+1.4}_{-1.2} \pm 0.3 \pm 0.3$
$[8,12]$	$15.7\,^{+5.3}_{-4.6} \pm 0.4$	$2.83 \pm 0.15 \pm 0.18$	$5.0\,^{+1.7}_{-1.5} \pm 0.2 \pm 0.1$
$[12,16]$	$12.7\,^{+4.7}_{-4.0} \pm 0.4$	$2.71 \pm 0.14 \pm 0.07$	$4.3\,^{+1.6}_{-1.4} \pm 0.2 \pm 0.1$
$[16,20]$	$16.0\,^{+5.1}_{-4.4} \pm 0.5$	$3.99 \pm 0.21 \pm 0.26$	$3.6\,^{+1.2}_{-1.0} \pm 0.2 \pm 0.2$

TABLE III: Yield, efficiency and branching fraction in each q^2 region. The first error is statistical, the second is systematic and the third is model dependence.

We thank the KEKB group for the excellent operation of the accelerator, the KEK Cryogenics group for the efficient operation of the solenoid, and the KEK computer group and the National Institute of Informatics for valuable computing and Super-SINET network support. We acknowledge support from the Ministry of Education, Culture, Sports, Science, and Technology of Japan and the Japan Society for the Promotion of Science; the Australian

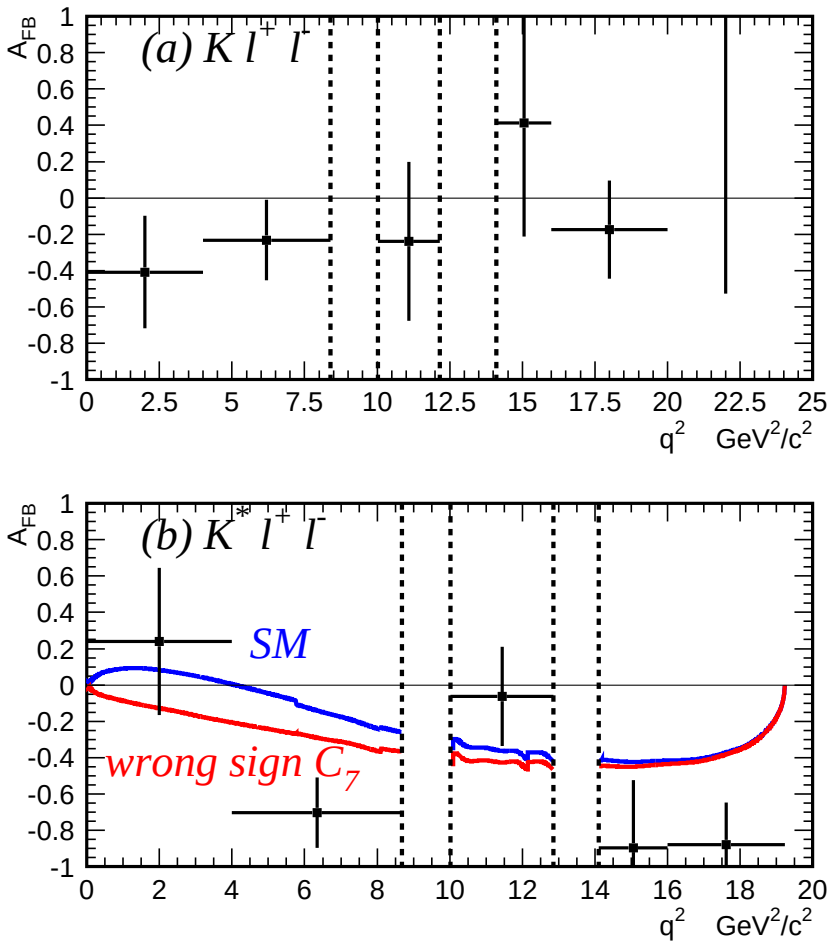

FIG. 3: The raw forward-backward asymmetry in (a) $K\ell^+\ell^-$ and (b) $K^*\ell^+\ell^-$. Points with error bars show the data. Curves show theoretical predictions including the effect of experimental efficiency and resolution for the SM case (blue) and wrong-sign C_7 case (red). The pairs of dashed lines are the boundaries of the J/ψ and ψ' veto regions.

Research Council and the Australian Department of Education, Science and Training; the National Science Foundation of China under contract No. 10175071; the Department of Science and Technology of India; the BK21 program of the Ministry of Education of Korea and the CHEP SRC program of the Korea Science and Engineering Foundation; the Polish State Committee for Scientific Research under contract No. 2P03B 01324; the Ministry of Science and Technology of the Russian Federation; the Ministry of Education, Science and Sport of the Republic of Slovenia; the National Science Council and the Ministry of Education of Taiwan; and the U.S. Department of Energy.

---

* on leave from Nova Gorica Polytechnic, Nova Gorica

[1] K. Abe *et al.* (Belle Collaboration), *Phys. Lett.* B **511**, 151 (2001).

[2] S. Chen *et al.* (CLEO Collaboration), *Phys. Rev. Lett.* **87**, 251807 (2001).
[3] R. Barate *et al.* (ALEPH Collaboration), *Phys. Lett.* B **429**, 169 (1998).
[4] T. Besmer, C. Greub, T. Hurth. CERN-TH-2001-136, BUTP-01-12, ZU-TH-15-01, hep-ph/0105292; M. Ciuchini *et al.*, *Nucl. Phys.* B **534**, 3 (1998); C. Bobeth, M. Misiak and J. Urban, *Nucl. Phys.* B **567**, 153 (2000); F. Borzumati *et al.*, *Phys. Rev.* D **62**, 075005 (2000); T. Goto *et al.*, *Phys. Rev.* D **58**, 094006 (1998).
[5] K. Abe *et al.* (Belle Collaboration), *Phys. Rev. Lett.* **88**, 021801 (2002).
[6] A. Ishikawa *et al.* (Belle Collaboration), *Phys. Rev. Lett.* **91**, 261601 (2003).
[7] J. Kaneko *et al.* (Belle Collaboration), *Phys. Rev. Lett.* **90**, 021801 (2003).
[8] A. Ali *et al.*, *Phys. Rev.* D **66**, 034002 (2002).
[9] E. Lunghi, arXiv:hep-ph/0210379.
[10] E. Lunghi *et al.*, *Nucl. Phys.* B **568**, 120 (2000); J. L. Hewett and J. D. Wells, *Phys. Rev.* D **55**, 5549 (1997); A. Ali, G. F. Giudice and T. Mannel, *Z. Phys.* C **67**, 417 (1995); N. G. Deshpande, K. Panose and J. Trampetić, *Phys. Lett.* B **308**, 322 (1993); A. Ali, T. Mannel and T. Morozumi, *Phys. Lett.* B **273**, 505 (1991); B. Grinstein, M. J. Savage and M. B. Wise, *Nucl. Phys.* B **319**, 271 (1991); W. S. Hou, R. S. Willey and A. Soni, *Phys. Rev. Lett.* **58**, 1608 (1987).
[11] S. Kurokawa and E. Kikutani, *Nucl. Instrum. Meth.* A **499**, 1 (2003), and other papers included in this Volume.
[12] A. Abashian *et al.* (Belle Collaboration), *Nucl. Instrum. Meth.* A **479**, 117 (2002).
[13] Y. Ushiroda (Belle SVD2 Group), *Nucl. Instrum. Meth.* A **511**, 6 (2003).
[14] Charge conjugate modes are implied throughout this paper.
[15] Throughout this paper, variables denoted with an asterisk are calculated in the $\Upsilon(4S)$ rest frame.
[16] R. A. Fisher, *Ann. Eugen.* **7**, 179 (1936); M. C. Kendall and A. Stuart, *The Advanced Theory of Statistics,* Second Edition (Hafner, New York, 1968) Vol III.
[17] G. Fox and S. Wolfram, *Phys. Rev. Lett.* **41**, 1581 (1978).
[18] D. Melikhov, N. Nikitin and S. Simula, *Phys. Lett.* B **410**, 290 (1997).
[19] P. Colangelo *et al.*, *Phys. Rev.* D **53**, 3672 (1998), Erratum-ibid.D **57**, 3186 (1998).
[20] H. Albrecht *et al.* (ARGUS Collaboration), *Phys. Lett.* B **241**, 278 (1990).
[21] M. Zhong, *et al. Int. J. Mod. Phys.* A **18**, 1959 (2003); T. M. Aliev, C. S. Kim, Y. G. Kim, *Phys. Rev.* D **62**, 014026 (2000); P. Colangelo *et al. Eur. Phys. J.* C **8**, 81 (1999); G. Burdman, *Phys. Rev.* D **52**, 6400 (1995); C. Greub, A. Ioannissian and D. Wyler, *Phys. Lett.* B **346**, 149 (1995); W. Jaus and D. Wyler, *Phys. Rev.* D **41**, 3405 (1990); N. G. Deshpande, J. Trampetić and K. Panose, *Phys. Rev.* D **39**, 1461 (1989); N. G. Deshpande and J. Trampetić, *Phys. Rev. Lett.* **60**, 2583 (1988).
[22] G. Hiller and F. Krüger, *Phys. Rev.* D **69**, 074020 (2004); Y. Wang and D. Atwood, *Phys. Rev.* D **68**, 094016 (2003).
[23] D. A. Demir, K. A. Olive and M. B. Voloshin, *Phys. Rev.* D **66**, 034015 (2002).